

Table 2 Bipedal gaits for a four-cell CPG network

Slow hop		Fast hop		Walk		Run	
0	0	$\frac{1}{2}$	$\frac{1}{2}$	$\frac{1}{2}$	0	0	$\frac{1}{2}$
0	0	0	0	0	$\frac{1}{2}$	0	$\frac{1}{2}$

in preparation), which are secondary gaits. Experimentally observed variability from exact quarter-period and half-period phase shifts^{21,22} can, in principle, be accounted for by analysing symmetry-broken secondary gaits. As the signals sent to fore legs in primary gaits are identical and in secondary gaits are unequal, the duty factors of the fore legs should be equal in primary gaits and unequal in secondary gaits. Indeed, the duty factors of fore legs of a walking horse are equal⁸ and those of a galloping horse are different^{23,24}.

Prediction 2. Table 1 includes a non-standard primary gait, the jump, which can be described as 'fore feet hit ground, then hind feet hit ground, then three beats later fore feet hit ground'. We observed a gait with that pattern in a bucking bronco. (A figure showing four equal-time-interval frames, taken from a video provided by The Houston Livestock Show and Rodeo of the bareback bronco event on 24 February 1999, is available electronically at ftp://ftp.math.uh.edu/pub/laode/rodeo.) The timing of the footfalls is close to 0 and 1/4 of the period of this rhythmic motion. The primitive ricocheting jump of a Norway rat and an Asia Minor gerbil also has this cadence⁶.

Prediction 3. We next predict the occurrence of half-integer wave numbers in myriapod gaits. Because the network has twice as many cells as the animal has legs, the number of waves of leg movement that fit into the observable half of the network is either an integer or half an odd integer. Manton²⁵ provides drawings of several centipede gaits; the number of waves is close either to an integer (4, 3, 2) or half an odd integer (3/2); see Fig. 2. The tripod gait of hexapods²⁶ is a 3/2 wave.

Prediction 4. Finally, we specialize the network to bipeds where hidden cells seem unnecessary⁹. For evolutionary reasons, we expect bipeds not to break the pattern hypothesized for many-legged animals, thus resulting in four primary bipedal gaits (Table 2). If hidden cells do occur in bipedal CPGs, they should play an active role, perhaps controlling the timing of different muscle groups. Thus, muscle groups may reveal the presence of two distinct gaits in which the legs move half a period out of phase. More precisely, lower leg muscles should be activated synchronously in one gait and asynchronously in the other—because of the phases of the hidden cells. The human gaits walk and run support this prediction^{27,28}. During walking, the gastrocnemius (an ankle plantarflexor) and the tibialis anterior (an ankle dorsiflexor) are activated out of phase, whereas during running, they are co-activated during significant portions of the gait cycle.

Unlike bipeds, the hidden phases of quadrupedal primary gaits can be deduced from the observable half network. Thus, each primary gait corresponds either to synchronous muscle activation (as in the run) asynchronous activation (as in the walk). This prediction should be testable. □

Received 21 May; accepted 9 August 1999.

- Delcomyn, F. Neural basis of rhythmic behavior in animals. *Science* **210**, 492–498 (1980).
- Grillner, S. Locomotion in vertebrates: central mechanisms and reflex interaction. *Physiol. Rev.* **55**, 247–304 (1975).
- Selverston, A. I. Are central pattern generators understandable? *Behav. Brain Sci.* **3**, 535–571 (1980).
- Shik, M. L. & Orlovsky, G. N. Neurophysiology of locomotor automatism. *Physiol. Rev.* **56**, 465–501 (1976).
- Alexander, R. McN. In *Mechanics and Energetics of Animal Locomotion* (eds Alexander, R. McN. & Goldspink, J. M.) 168–203 (Chapman and Hall, London, 1977).
- Gambaryan, P. P. *How Mammals Run: Anatomical Adaptations* (Wiley, New York, 1974).
- Hildebrand, M. Symmetrical gaits of horses. *Science* **150**, 701–708 (1965).
- Hildebrand, M. The quadrupedal gaits of vertebrates. *Bioscience* **39** (11) 766–775 (1989).
- Collins, J. J. & Stewart, I. Coupled nonlinear oscillators and the symmetries of animal gaits. *J. Nonlin. Sci.* **3**, 349–392 (1993).

- Golubitsky, M., Stewart, I., Buono, P. L. & Collins, J. J. A modular network for legged locomotion. *Physica D* **115**, 56–72 (1998).
- Schöner, G., Jiang, W. Y. & Kelso, J. A. S. A synergetic theory of quadrupedal gaits and gait transitions. *J. Theor. Biol.* **142**, 359–391 (1990).
- Collins, J. J. & Stewart, I. Symmetry-breaking bifurcation: a possible mechanism for 2:1 frequency-locking in animal locomotion. *J. Math. Biol.* **30**, 827–838 (1992).
- Collins, J. J. & Stewart, I. Hexapodal gaits and coupled nonlinear oscillator models. *Biol. Cybern.* **68**, 287–298 (1993).
- Collins, J. J. & Stewart, I. A group-theoretic approach to rings of coupled biological oscillators. *Biol. Cybern.* **71**, 95–103 (1994).
- Kopell, N. & Ermentrout, G. B. Symmetry and phaselocking in chains of weakly coupled oscillators. *Comm. Pure Appl. Math.* **39**, 623–660 (1986).
- Kopell, N. & Ermentrout, G. B. Coupled oscillators and the design of central pattern generators. *Math. Biosci.* **89**, 14–23 (1988).
- Kopell, N. & Ermentrout, G. B. Phase transitions and other phenomena in chains of oscillators. *SIAM J. Appl. Math.* **50**, 1014–1052 (1990).
- Buono, P.-L. & Golubitsky, M. Models of central pattern generators for quadruped locomotion: I. primary gaits. *J. Math. Biol.* (submitted).
- Golubitsky, M., Stewart, I. N. & Schaeffer, D. G. *Singularities and Groups in Bifurcation Theory* Vol. 2 275–282 387–399 (Springer, New York, 1988).
- Buono, P.-L. *A Model of Central Pattern Generators for Quadruped Locomotion*. PhD Thesis, Mathematics Department, Univer. Houston (1998).
- Hildebrand, M. in *Neural Control of Locomotion* (eds Herman, R. M., Grillner, S., Stein, P. S. G. & Stewart, D. G.) 203–236 (Plenum, New York, 1976).
- Alexander, R. McN. & Jayes, A. S. A dynamic similarity hypothesis for the gaits of quadrupedal mammals. *J. Zool.* **201**, 135–152 (1983).
- Leach, D. H. & Spriggs, E. Gait fatigue in the racing thoroughbred. *J. Equine Med. Surg.* **3**, 436–443 (1979).
- Deuel, N. R. & Lawrence, L. M. Laterality in the gallop gait of horses. *J. Biomech.* **20**, 645–649 (1987).
- Manton, S. M. The evolution of arthropod locomotory mechanics. Part 8: Functional requirements and body design in Chilopoda. *J. Linnaean Soc. (Zool.)* **45**, 251–484 (1965).
- Full, R. J., Blickhan, R. & Ting, L. H. Leg design in hexapedal runners. *J. Exp. Biol.* **158**, 369–390 (1991).
- Mann, R. A. in *Disorders of the Foot* (ed. Jahss, M. H.) 37–67 (W. B. Saunders, Philadelphia, 1982).
- Mann, R. A., Moran, G. T. & Dougherty, S. E. Comparative electromyography of the lower extremity in jogging, running and sprinting. *Am. J. Sports Med.* **14**, 501–510 (1986).

Acknowledgements

We thank A. Golubitsky for help in analysing the jump gait from the rodeo video, kindly supplied by the Houston Livestock Show and Rodeo. We also thank Ray Glantz for discussions. This research was supported in part by grants from the NSF and the Texas Advanced Research Program.

Correspondence and requests for materials should be addressed to M.G. (e-mail: mg@uh.edu).

Probing the human stereoscopic system with reverse correlation

Peter Neri, Andrew J. Parker & Colin Blakemore

University Laboratory of Physiology, Parks Road, Oxford OX1 3PT, UK

Our two eyes obtain slightly different views of the world. The resulting differences in the two retinal images, called binocular disparities, provide us with a stereoscopic sense of depth¹. The primary visual cortex (V1) contains neurons that are selective for the disparity^{2–4} of individual elements in an image, but this information must be further analysed to complete the stereoscopic process^{5,6}. Here we apply the psychophysical technique of reverse correlation⁷ to investigate disparity processing in human vision. Observers viewed binocular random-dot patterns, with 'signal' dots in a specific depth plane plus 'noise' dots with randomly assigned disparities. By examining the correlation between the observers' ability to detect the plane and the particular sample of 'noise' disparities presented on each trial, we revealed detection 'filters', whose disparity selectivity was remarkably similar to that of individual neurons in monkey V1. Moreover, if the noise dots were of opposite contrast in the two eyes, the

tuning inverted, just like the response patterns of V1 neurons^{5,6}. Reverse correlation appears to probe disparity processing at the earliest stages of binocular combination, prior to the generation of a full stereoscopic depth percept.

Subjects viewed random-dot stereograms⁸ that depicted a background surface with the same disparity as the binocular fixation point, and a central square that was either in the same plane as the background (zero disparity) or standing forward from the background (target disparity). Their task was to report the absence or presence of the target plane (Fig. 1a). An additional disparity drawn from a discrete uniform distribution (a random value within a certain fixed range of disparities; Fig. 1b and Methods) was added to a fraction of the dots in the central square region, whether this region stood forward or not. This made the task much more difficult, requiring the observer to make perceptual decisions about the depth of the signal dots in the central region in the presence of a cloud of interfering noise dots, all at different depths.

A preliminary experiment determined that adding such disparity noise to 95% of the dots in the central region brought detection performance down to about 75% correct. A large number of trials (10,000–15,000) were conducted with these near-threshold stimuli. The actual profile of disparity values in the central region varied from trial to trial owing to the random sampling procedure: some of these variations in the noise distribution had no effect on detection performance, but others were highly influential. We hypothesized that configurations of the noise that affected the detection task would reveal the properties of mechanisms normally involved in the processing of disparity.

After each trial, the computer recorded the number of noise dots at each disparity level, the presence or absence of the target and the observer's response. These individual noise distributions were separately averaged for each possible class of response—hit, false alarm, miss and correct rejection (Fig. 1c and Methods; see also ref. 7). Within each noise pattern, 50% of the dots had same-contrast polarity, dark or bright, in both eyes (binocularly correlated) and 50% had opposite-contrast polarity in each eye (binocularly anti-correlated). The four averages of noise distributions were computed separately for binocularly correlated and anti-

correlated noise dots. (We obtained results similar to those presented here when the effect of each type of binocular correlation was explored independently in individual blocks of trials.) The process of computing the averages separately for each class of psychophysical response allowed us to analyse whether the particular distribution of disparity noise on each trial assisted or hindered the detection of the stereo target. Not surprisingly, 'yes' responses (hits and false alarms) were more common, and 'no' responses less frequent, when there was, by chance, an excess of same-contrast noise dots close to the target depth plane.

Figure 2 shows the summed profiles of noise as a function of disparity for both same-contrast (correlated) and reversed-contrast (anti-correlated) noise dots, for two observers. Correlated noise yields a function with a positive peak at the disparity of the target and clear negative flanks at each side, broadly similar to those derived with other psychophysical techniques^{9,10}. Binocular neurons in primate V1 produce similar functions when their firing rate is measured for stimuli of different disparity^{2–4}. Interestingly, the summed profile for anti-correlated noise (reversed-contrast) generates a roughly opposite profile: there is a small, but distinct, trough at the disparity of the target. Many V1 neurons respond in this way to anti-correlated random-dot stereograms: their response profile is inverted, but of smaller modulation, compared with that for patterns with same contrast in each eye⁶. It is interesting that anti-correlated stimuli can drive vergence eye movements in the geometrically inappropriate direction: an anti-correlated target that steps away from the observer in terms of retinal disparity actually induces a transient convergent eye movement¹¹.

Disparity-selective neurons in the striate cortex have been modelled as units that correlate one-dimensional Gabor-filtered images arriving from each eye^{5,6}. We subjected a synthetic detector of this type to the same experimental procedure used in the psychophysical experiment (Fig. 3a), using exactly the same values for the parameters. No rescaling was applied to the resulting simulations of the detection curves. Figure 3b shows how this model captures all aspects of the psychophysical results, with one noticeable exception: the simulated amplitude of the function for anti-correlated noise is larger than experimentally observed. In reality, this discrepancy

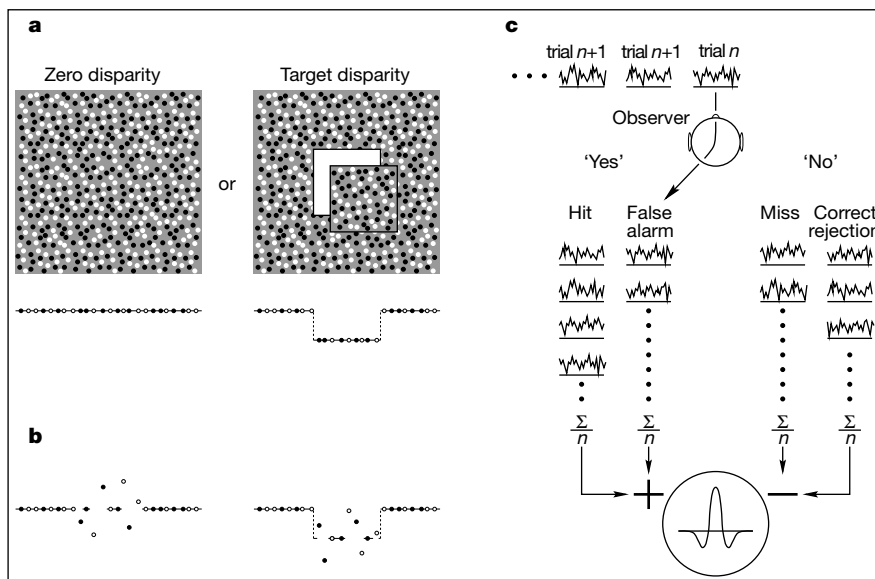


Figure 1 Psychophysical task and reverse-correlation technique. **a**, Random-dot stereograms (front views and top views shown) either contained or did not contain a disparity-defined central square (target). **b**, Observers were required to detect the target, while disparity noise was added to the central region. **c**, Noise configurations for a sequence of threshold stimuli (top row: noise density * as a function of disparity) were

classified according to the observer's response. Summation of average noise distributions yielding 'yes' responses (hits and false alarms) and subtraction of those giving 'no' responses (misses and correct rejections) generates the presumed disparity-selective sensory filter (response versus disparity).

highlights the similarity of psychophysical and neurophysiological results: neurons in monkey V1 and human psychophysical detection functions both exhibit a relatively reduced amplitude of modulation for anti-correlated stimuli. Qualitatively, the inversion of the function for reversed-contrast stimuli is expected from any mechanism that preserves the polarity of the Gabor-filtered inputs. The smaller amplitude might be explained by some threshold or saturating nonlinearity in the contrast-response functions of the underlying monocular filters. For binocularly correlated noise, this simple model gives reasonably accurate predictions of human performance, chiefly because we introduced a large amount of external noise, which dominates the statistical level of performance for both human observers and the model. As the synthetic unit did not have any internal noise, one can conclude that the effect of any internal neural noise in the human observers was also relatively slight in these circumstances.

These results provide important clues about the way in which the neural processing of binocular disparity leads to the perception of stereoscopic depth. Dense anti-correlated random-dot stereograms elicit responses (albeit inverted in modulation) from binocular neurons in early visual areas⁶ but such stimuli do not support stereoscopic vision^{8,12-14}. Sparse stereograms and single bars of opposite contrast in the two eyes can provide a weak impression of depth^{12,13}, but when stereopsis occurs, it is at a depth consistent with the retinal disparity of the contrast-reversed elements¹⁴. From these perceptual observations, one would expect the anti-correlated response function in the present experiments to be qualitatively similar in form to that for correlated noise, rather than inverted as in Fig. 2.

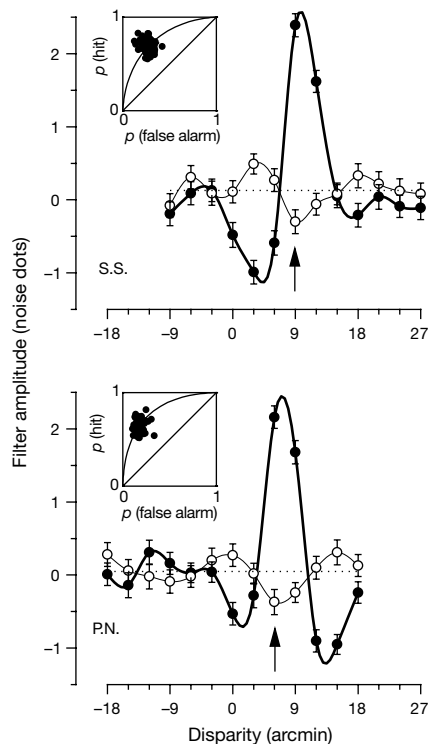


Figure 2 Tuning functions for two observers (top, observer S.S., 11,000 trials; bottom, observer P.N., 13,000 trials). Solid symbols (± 1 s.e.) and thick splines plot response functions for binocular contrast-correlated noise; open symbols (thin splines) plot functions for anti-correlated noise. Dotted lines are mean values. Arrows indicate target disparity: 9 arcmin for S.S. and 6 arcmin for P.N. Correlated noise yields a Mexican-hat-shaped function; anti-correlated noise an inverted pattern of smaller amplitude. The insets plot probability of hit against probability of false alarm; each dot refers to an individual block. Smooth curves plot a constant level of performance in terms of d' (see Methods). Average d' values were 1.1 (S.S.) and 1.3 (P.N.).

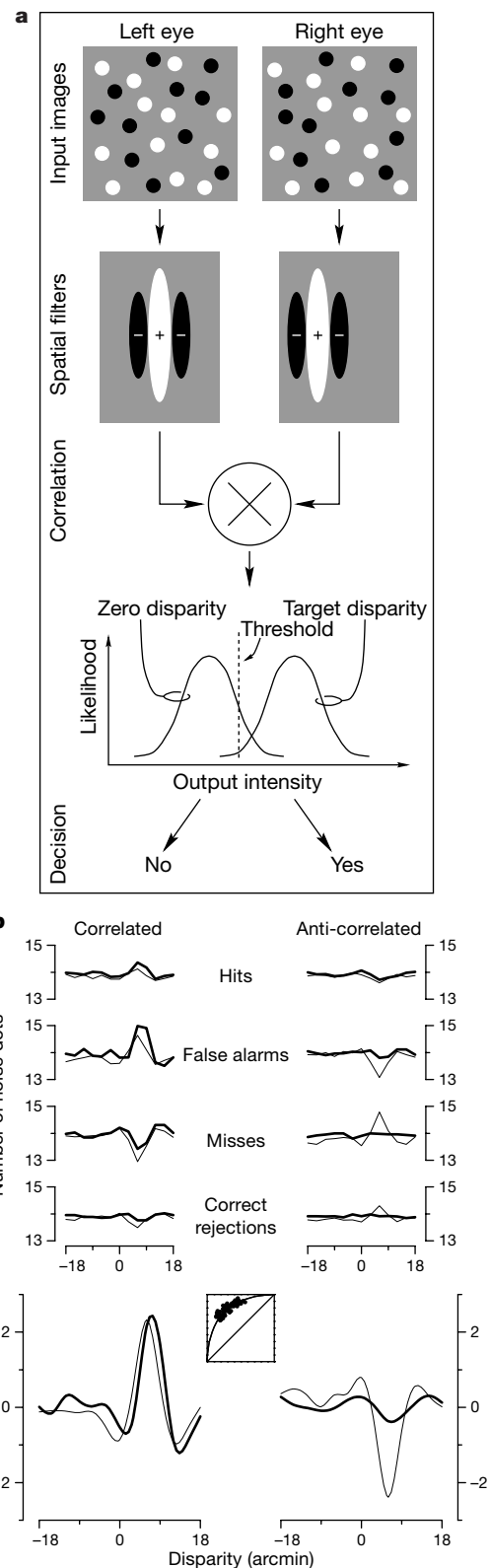


Figure 3 Model and simulation of data. **a**, The synthetic detector consisted of two monocular spatial filters, offset to a characteristic preferred disparity, whose outputs were correlated to yield the response^{5,6}. This was converted to a binary choice. **b**, The detector was challenged with stimulus images used for the psychophysics, and the reverse-correlation technique applied. Thick lines summarize experimental data for subject P. N.; thin lines are the corresponding simulation curves. Average noise configurations for all four stimulus-response classes are shown (upper part), as is the combined disparity-tuning function (lower part). The model reproduces most experimental features (including d' scores, shown in the central inset: conventions as in Fig. 2), apart from the reduced amplitude of the function for anti-correlated noise.

This raises the following question: given that anti-correlated stimuli alone lead to either a weak percept of correct depth or a percept of no depth at all, how is it that anti-correlated noise reduces the detectability of binocularly correlated stimuli when at the same disparity and enhances detectability when at neighbour disparities? The answer may lie in the stage of processing that is probed by the detection task used here. At the earliest stage of binocular combination, inputs from the left and right eyes seem to be combined almost linearly^{5,6}. Such a mechanism would provide for an interaction between the binocularly correlated stimulus and the anti-correlated noise dots. The data presented here show that this stage can be identified psychophysically by the reverse-correlation technique⁷. This powerful new tool may be of general value in revealing the properties of low-level perceptual mechanisms.

Our results provide insights into how the perception of depth arises in the human visual system. We can now identify at least two separate stages in the generation of a full stereoscopic percept. In the initial stage, information from the two eyes is combined in a local, feature-specific manner². This process is close to a measurement of binocular correlation, thus exhibiting an inverted response when anti-correlated stimuli are used. This stage, perhaps occurring in human V1, appears to support the basic detection task in this study. At a later stage, the detailed matching of information between the two eyes is sorted out on a broader scale. The overall binocular correspondence problem is solved to yield the perception of surfaces and boundaries in depth from potentially multiply ambiguous local cues^{15,16}. If our speculation that V1 holds the initial stage of binocular combination is correct, it remains to identify the site or sites where true stereoscopic correspondence is established and signals from dense, globally anti-correlated patterns are rejected. □

Methods

Stimuli were generated by a VSG graphics card (CRS, Rochester, UK) and presented on a CRT monitor (Vision Master 17, Iiyama) at a viewing distance of 57 cm. To provide independent stimulation of the eyes, the graphics card was synchronized with ferroelectric stereo-goggles at 110 Hz (55 Hz for each eye). The observer fixated a central red cross, presented to both eyes (zero disparity), against a grey background (35 cd m⁻²). This cross disappeared during the 250-ms presentations of a stereogram subtending 11.5° × 11.5°. Each stereogram consisted of randomly distributed dots (6 arcmin diameter; density 12%), half of which were bright (65 cd m⁻²) and half dark (5 cd m⁻²), on the same grey background so that stimulus onset did not change mean luminance.

The periphery of all stereograms consisted entirely of correlated dots at zero disparity, perceived as a background surface. Within a central square (5.8° × 5.8°), the signal dots all had the same disparity, either zero (forming a surface continuous with the background), or a target disparity (6 arcmin crossed disparity for one subject, 9 arcmin for the other, corresponding to a square surface, closer than the background). The disparity of the other dots in the central region was drawn randomly from a discrete uniform distribution, spanning 13 disparity levels of 3 arcmin steps, centred around either the target disparity (subject S.S.) or zero disparity (subject P.N.). Half the noise dots in each stereogram were matched in contrast in the two eyes (both either dark or bright); the others were of opposite contrast (one dark and one bright). They were painted alternately, so that there was an equal probability that correlated noise dots would be occluded by anticorrelated and vice versa. Signal dots were evenly interspaced among noise dots in the drawing sequence.

At the end of each presentation, the observer made a forced-choice decision about whether signal dots were at the target disparity. This decision triggered the next presentation after a 500-ms delay. Every 30–50 trials, a target square without noise was presented so as to remind the observer of its appearance and to help to maintain vigilance. Subject S.S. was naive of the goals and methodology of the study.

Estimation of noise tolerance threshold

In signal-detection theory¹⁷, the parameter d' provides a dimensionless measure of the detectability of a stimulus, expressing signal strength as a multiple of the standard deviation of the underlying probability distribution of the detection process. During these experiments, the stimulus always had 95% noise dots and 5% signal dots, which yielded $d' \sim 1.2$. These values were estimated from a preliminary block of ~200 trials during which the fraction of noise dots was adjusted up or down after each trial¹⁸.

Reverse-correlation analysis

Our technique was adapted from that developed by Beard and Ahumada⁷ for a Vernier task. Blocks consisted of 200 trials. The disparity distribution of noise dots for each presentation was stored and sorted according to which response class had occurred (hit, false alarm, miss or correct rejection). Noise distributions were averaged to obtain the

mean noise configuration associated with each response. By summing the average configurations for the 'yes' responses (hits and false alarms) and subtracting those for the 'no' responses (misses and correct rejections), we obtained the single tuning function for the presumed sensory filter used to perform the task (Fig. 1c).

Estimates of variance for the data points in Fig. 2 were obtained with a bootstrap method¹⁹, in which random picks (with replacement) were repeatedly taken from the experimentally obtained data sets according to a pattern that matched the actual distribution of classes of response produced during the experiment. 1,000 samples of these synthetic data were subjected to the same analysis procedure used for the true data. This generates a bootstrap estimate of the sampling distribution of the values plotted in Fig. 2. The error bars show ± 1s.e.

Modelling

We used a synthetic detector similar to that of Ohzawa *et al.*⁵, but with the two monocular receptive fields extended to both spatial dimensions (Fig. 3a). Stimulus images, generated exactly as for the experiments, were filtered by x -Gabor/ y -gaussian filters, which had a disparity offset (the preferred disparity for the detector), and sampled the image at a number of different positions (i, j in the equation below). We chose a position-disparity model (as opposed to phase disparity) because the spatial frequency of the filter (see below) was well above 2.5 cycles per deg (ref. 20).

$$\text{Output} = \sum_{ij} \left[\sum_{xy} f_R(x, y) I_R(x + i, y + j) \right] \cdot \left[\sum_{xy} f_L(x, y) I_L(x + i, y + j) \right]$$

where $I(i, j)$ is the image, R and L refer to the eyes, and the filter f is of the form:

$$f(x, y) = \cos(\omega x) G(x, \sigma_x) G(y, \sigma_y)$$

where G is a gaussian function of standard deviation σ ($\sigma_x = 3 \text{ arcmin}$, $\sigma_y = 1.5^\circ$, $\omega = 5$ cycles per deg for Fig. 3b). The output was converted into a yes–no response by a statistical thresholding procedure (Fig. 3a, bottom). The reverse-correlation technique was applied to the outputs of this synthetic detector to generate response functions like those obtained in the psychophysical experiments.

Received 7 May; accepted 16 August 1999.

1. Wheatstone, C. Contributions to the physiology of vision—Part the first. On some remarkable and hitherto unobserved phenomena of binocular vision. *Phil. Trans. R. Soc.* **128**, 371–394 (1838).
2. Barlow, H. B., Blakemore, C. & Pettigrew, J. D. The neural mechanism of binocular depth discrimination. *J. Physiol. (Lond.)* **193**, 327–342 (1967).
3. Nikara, T., Bishop, P. O. & Pettigrew, J. D. Analysis of retinal correspondence by studying receptive fields of binocular single units in cat striate cortex. *Exp. Brain Res.* **6**, 353–372 (1968).
4. Poggio, G. F. & Fischer, B. Binocular interaction and depth sensitivity in striate and prestriate cortex of behaving Rhesus monkey. *J. Neurophysiol.* **40**, 1392–1407 (1977).
5. Ohzawa, I., DeAngelis, G. C. & Freeman, R. D. Stereoscopic depth discrimination in the visual cortex: neurons ideally suited as disparity detectors. *Science* **249**, 1037–1041 (1990).
6. Cumming, B. G. & Parker, A. J. Responses of primary visual cortical neurons to binocular disparity without depth perception. *Nature* **389**, 280–283 (1997).
7. Beard, B. L. & Ahumada, A. J. Jr in *Human Vision and Electronic Imaging III* (eds Rogowitz, B. E. & Pappas, T. N.) *Proc. SPIE* **3299**, 79–85 (1998).
8. Julesz, B. *Foundations of Cyclopean Perception* (Univ. Chicago Press, 1971).
9. Stevenson, S. B., Cormack, L. K., Schor, C. M. & Tyler, C. W. Disparity tuning in mechanisms of human stereopsis. *Vision Res.* **32**, 1685–1694 (1992).
10. Cormack, L. K., Stevenson, S. B. & Schor, C. M. Disparity-tuned channels of the human visual system. *Vis. Neurosci.* **10**, 585–596 (1993).
11. Masson, G. S., Busetini, C. & Miles, F. A. Vergence eye movements in response to binocular disparity without depth perception. *Nature* **389**, 283–286 (1997).
12. Cogan, A. I., Kontsevich, L. L., Lomakin, A. J., Halpern, D. L. & Blake, R. Binocular disparity processing with opposite-contrast stimuli. *Perception* **24**, 33–47 (1995).
13. Cogan, A. I., Lomakin, A. J. & Rossi, A. F. Depth in anti-correlated stereograms: effects of spatial density and interocular delay. *Vision Res.* **33**, 1959–1975 (1993).
14. Cumming, B. G., Shapiro, S. E. & Parker, A. J. Disparity detection in anticorrelated stereograms. *Perception* **27**, 1367–1377 (1998).
15. Marr, D. & Poggio, T. A computational theory of human stereo vision. *Proc. R. Soc. Lond. B* **204**, 301–328 (1979).
16. Fleet, D. J., Wagner, H. & Heeger, D. J. Neural encoding of binocular disparity: energy models, position shifts and phase shifts. *Vision Res.* **36**, 1839–1857 (1996).
17. Green, D. M. & Swets, J. A. *Signal Detection Theory and Psychophysics* (Wiley, New York, 1966).
18. Watson, A. B. & Pelli, D. G. QUEST: a Bayesian adaptive psychometric method. *Percept. Psychophys.* **33**, 113–120 (1983).
19. Efron, B. & Tibshirani, R. *An Introduction to the Bootstrap* (Chapman & Hall, New York, 1993).
20. Schor, C., Wood, I. & Ogawa, J. Binocular sensory fusion is limited by spatial resolution. *Vision Res.* **24**, 661–665 (1984).

Acknowledgements

We thank H. Barlow and B. Cumming for comments. This work was supported by the Oxford McDonnell–Pew Centre for Cognitive Neuroscience, the Medical Research Council and the Wellcome Trust.

Correspondence and requests for materials should be addressed to P.N. (e-mail: peter.neri@physiol.ox.ac.uk).